Short Scan Source-detector Trajectories for Target-based CBCT

Sepideh Hatamikia*, Ander Biguri, Gernot Kronreif, Tom Russ, Joachim Kettenbach, Wolfgang Birkfellner

***Abstract*— We proposed a target-based cone beam computed tomography (CBCT) imaging framework in order to optimize a free three dimensional (3D) source–detector trajectory by incorporating prior 3D image data. We aim to enable CBCT systems to provide topical information about a region of interest (ROI) using a short-scan trajectory with a reduced number of projections. The best projection views are selected by maximizing an objective function fed by the image quality by means of applying different x-ray positions on the digital phantom data. Finally, an optimized trajectory is selected which is applied to a C-arm device able to perform general source–detector positioning. An Alderson-Rando head phantom is used in order to investigate the performance of the proposed framework. Our experiments showed that the optimized trajectory could achieve a comparable image quality in the ROI with respect to the reference C-arm CBCT while using approximately one-quarter of projections. An angular range of 156° was used for the optimized trajectory.**

I. Introduction

Nowadays, cone beam computed tomography (CBCT) has become an important tool for interventional three dimensional (3D) imaging as well as patient setup and dose verification in external beam radiotherapy [1]. In conventional CBCT, a circular isocentric source-detector trajectory is used to acquire 2D projections in order to reconstruct a 3D volume. However, this standard methodology introduces a couple of limitations. The number of projections in conventional CBCT is high and introduces a considerable radiation dose to the patient. In particular for the repetitive use of CBCT in an image-guided procedure as well as for daily pretreatment patient alignment in radiotherapy, the accumulated radiation dose has become a concern [2] and dose reduction is always an important topic both for health care providers and patients. Another limitation regarding the circular trajectory is that rotation is limited around the patient cranio-caudal axis which sacrifices the information to be achieved from oblique viewing angles. Some studies tried to address this by employing non-conventional trajectories. In [3], the authors examined the integration of prior 3D imaging data for developing customized trajectories using a greedy approach as the trajectory optimization method. Non-circular trajectories are proposed in [4] using B-spline and periodic base functions in simulation experiments as well as in the neuroradiology [5]. Their proposed task-driven trajectories [3-5] could increase the reconstruction performance for a variety of imaging tasks. Another limitation of a circular trajectory corresponds to its wide angular range. Repetitive intraoperative 3D scans are needed in the operating theater and complex interventions often require multiple complete C-arm gantry rotations around the patient. In this case, the wide angular range needed for a circular trajectory can be problematic due to the geometric constraints related to the imaging device, patient positioning table and operation room. Robotic surgery is another example in which there is a possibility of collision between the robot mounted on the table and the imaging machine. In these cases, CBCT reconstruction from a limited-angle view data is of potential advantage [6-8]. One important feature of interventional radiology and radiotherapy is that the region of interest (ROI) is known from high-resolution pre-treatment imaging. Thus, prior knowledge of patient anatomy and the ROI is available. The aim of this study is to incorporate such prior information into a customized CBCT trajectory by finding a source-detector trajectory with optimal orientation and minimal projection number in order to sufficiently image the ROI. For this aim we take advantage of unconventional imaging angles by incorporating partial rotations in 3D space. The resulting trajectory can minimize the radiation dose and is suitable for limited angle CBCT reconstruction. We developed a new feature for the open source Tomographic Iterative GPU-based Reconstruction (TIGRE) toolkit [9] to enable reconstruction based on arbitrary 3D source-detector trajectories.

II. Materials and Methods

A. Workflow of the customized CBCT

The suggested custom-designed CBCT imaging workflow is showed in Fig. 1. In this study, a patient-specific model from prior CT is acquired and used as the digital phantom for the trajectory simulations. In the simulation phase, a set of possible x-ray source-detector trajectories are defined regarding the mechanical constraints of the imaging device. Then, synthetic 2D projections corresponding to each trajectory are generated from the CT-based digital phantom and a 3D image is reconstructed based on those simulated projections. Afterwards, an optimized trajectory is selected among the simulated trajectories (Section. C). Finally, the selected trajectory is applied on the C-arm device in the real

*Research is supported by ACMIT – Austrian Center for Medical Innovation and Technology.

S. Hatamikia is with ACMIT and Medical University of Vienna (MUV) (phone:+4366565293677; e-mail: sepideh.hatamikia@acmit.at).
A. Biguri is with Institute of Nuclear Medicine, University College London.
G. Kronreif is with ACMIT.
T. Russ is with Medical Faculty Mannheim, Heidelberg University.
J. Kettenbach is with Radiology and Nuclear Medicine Department in Wiener Neustadt hospital, Austria.
W. Birkfellner is with MUV.

situation to acquire real projections in order to perform reconstruction.

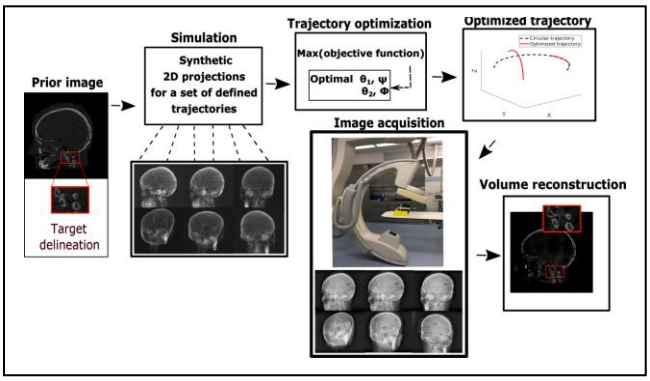

Figure 1. Diagram of the workflow for our proposed customized CBCT.

The proposed CBCT workflow was evaluated using a head Alderson-Rando phantom. We used the neck (C1/C2 region of the cervical spine) as an anatomical target for the experiments.

B. *Imaging device*

A Philips Allura FD20 Xper C-arm is used in this study. Source-detector and source-axis distances for the Philips C-arm are 1195 mm and 810 mm, respectively. The detector size is 26 x 38 cm with 0.776 mm pixel pitch. This C-arm is able to rotate by angle θ_1 towards Right Anterior Oblique (RAO)/Left Anterior Oblique (LAO) while having an oblique ψ in Cranial (CRA)/Caudal (CAU) direction. It is also able to rotate by angle θ_2 toward CRA /CAU direction and have an oblique φ in RAO/LAO direction.

C. *Trajectory optimization method*

In this study, we use a greedy approach similar to [3] to propose a two-level optimization method in order to investigate the optimal trajectory for a specific target. The optimization algorithm tries to find the best combination of two small arcs with optimized orientation in 3D space. In the first level of optimization, the best arc is selected among a group of pre-defined arcs by maximizing an objective function value. In the second level of optimization, the second best arc is selected among the same group of pre-defined arcs but in the way that its combination with the first arc leads to the maximum objective function value. The objective function is a measure of the reconstructed image quality which is calculated at the ROI of the image reconstructed from the simulated projections. The final optimized trajectory includes two arcs and offers the best image quality for the reconstructed image in the ROI among all pre-defined trajectories. For this aim, we define 237 small arcs (112 RAO/LAO arcs with CRA/CAU oblique +125 CRA/CAU arcs with RAO/LAO oblique) in total which are possible on the device geometry. Each small arc includes between 30 to 40 projections (in dependence on the table collision constraints) by sampling every other degree, resulting in an angular range between 60°-80°. All pre-defined arcs are represented in Fig. 2 with different colors.

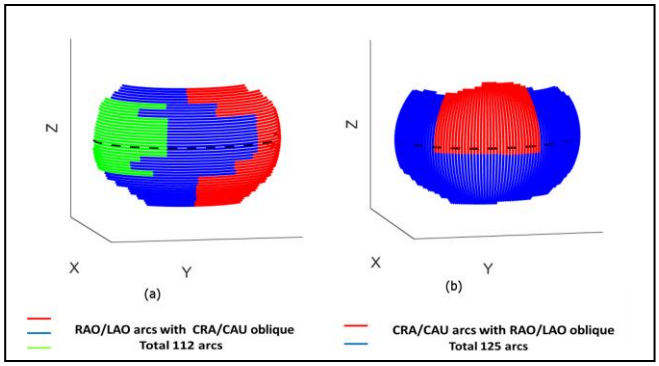

Figure 2. Pre-defined arcs for the trajectory optimization algorithm. The black dashed curve indicates the standard C-arm circular trajectory.

C.1. *Projection simulations*

In order to simulate CBCT data, synthetic projections are generated from the CT image of the head phantom. No additional noise was added to the simulated projections, as the CT scans are inherently noisy. System geometry is set to a source-detector distance of 1195 mm and a source-axis distance of 810 mm, approximating the geometry of the Philips C-arm. In addition, all simulated projections include 512 x 512 pixels and a 26 x 38 cm^2 detector size with 0.776 mm pixel pitch according to the real device detector specifications.

C.2. *Modification of the TIGRE toolbox for unconventional 3D source-detector trajectories*

One of the important achievement of our work is the modification of TIGRE toolbox to enable forward and backward projections and reconstruction based on unconventional trajectories with arbitrary 3D orientations. We enabled the TIGRE toolkit to perform reconstruction based on variety of non-isocentric/ arbitrary trajectories and presented our results at a recent conference [10]. We calculated the matrix R for z-y-z convention for Euler angles by multiplication of three intrinsic rotations as follows:

$$z.y'.z'', \quad \begin{bmatrix} c_{y'}c_{z''} - s_z s_{z''} & -c_{z''}s_z - c_z c_{y'} s_{z''} & c_z s_{y'} \\ c_z s_{z''} + c_{y'} c_{z''} s_z & c_z c_{z''} - c_{y'} s_z s_{z''} & s_z s_{y'} \\ -c_{z''} s_{y'} & s_{y'} s_{z''} & c_{y'} \end{bmatrix} = R \qquad (1)$$

where c and s are cos and sin, respectively. And successive orientations are denoted as follows: $x/y/z$ (initial), $x'/y'/z'$ (after first rotation) and $x''/y''/z''$(after second rotation). The resulting code is released freely available at https://github.com/CERN/TIGRE/releases/tag/v1.3.

C.3. *Objective function*

For the trajectory optimization procedure, we used Structural SIMilarity Index (SSIM) as the objective function to evaluate the performance of the reconstruction image obtained from the simulated projections. The SSIM tries to quantify the structural similarity of two images s and r based on luminance, contrast as well as structure [11]:

$$\mathrm{SSIM}(s,r) = \frac{(2\mu_s\mu_r + T_1)(2cov(s,r) + T_2)}{(\mu_s^2 + \mu_r^2 + T_1)(\sigma_s^2 + \sigma_r^2 + T_2)}, \qquad (2)$$

where $\mu_{s,r}$, $\sigma_{s,r}$ and $cov(s,r)$ correspond to the respective mean, variance and covariance values of the images. The

variables T_i include the dynamical range of the pixel values. The SSIM is comparing the reconstructed CBCT image obtained from the simulated projections and the prior knowledge CT. The image quality metric is calculated between both images after cropping them to contain the neck target (44×48×52 subset of voxels). A higher value of SSIM closer to 1 shows higher similarity between images.

C.4. Image reconstruction

We modified the codes related to the forward and backward projectors in TIGRE to include complex rotations therefore enabling iterative reconstruction algorithms with non-standard trajectories (Section C.2). Afterward, we used Adaptive steepest descent projection onto convex sets (ASD-POCS) algorithm implemented in TIGRE for the reconstruction based on both simulated and the real data. ASD-POCS was selected as reconstruction algorithm for this study due to its well-known robustness at low angular limited range sampling scanning trajectories [12]. In-house experiments also confirmed this. A 256^3 voxel volume (with 1 mm^3 voxels) was reconstructed for all experiments.

D. Real data image quality evaluation

In order to evaluate the image quality of the reconstructed ROI based on the real data, the following two metrics are used in our study:

1) Universal Quality Image (UQI) [13] which is defined as follows:

$$\mathrm{UQI} = \frac{2cov(s,r)}{\sigma_s^2+\sigma_r^2}\cdot\frac{2\mu_s\mu_r}{{\mu_s}^2+{\mu_r}^2} \quad (3)$$

where $\mu_{s,r}$, $\sigma_{s,r}$ and cov correspond to the mean, variance and covariance of the images. The UQI value is between 0 and 1 and increases with similarity.

2) Feature SIMilarity Index (FSIM) [14] which tries to calculate the distortion of important low level features. It is calculated based on phase congruency (PC) and gradient magnitude (GM) maps between two images s and r. Their similarity (S_{PC}, S_{GM}),

$$S_{PC}(s,r) = \frac{2PC_r\cdot PC_s+T_{PC}}{PC_r^2+PC_s^2+T_{PC}} \quad (4)$$

$$S_{GM}(s,r) = \frac{2GM_r\cdot GM_s+T_{GM}}{GM_r^2+GM_s^2+T_{GM}} \quad (5)$$

is calculated followed by their combination by using the PC as a weighting function:

$$\mathrm{FSIM}=\frac{\sum_{s,r\in\Omega} S(\mathrm{S_{PC}},\mathrm{S_{GM}})\cdot \mathrm{PC}_m(s,r)}{\sum_{s,r\in\Omega}\mathrm{PC}_m(s,r)}, \quad (6)$$

where T_{PC} and T_{GM} are values which are computed depending on the dynamic range of PC and GM. $\mathrm{PC}_m(s,r) = \max[\mathrm{PC}(s),\mathrm{PC}(r)]$ and Ω relates to the whole image spatial domain. FSIM has a value between 0 and 1 which increases with similarity.

III. RESULTS

The optimized trajectory is investigated in the simulations using a CT scan of the head phantom. After performing the trajectory optimization, the optimized trajectory for the neck target was selected. In order to demonstrate the importance of the correct orientation, we compared the CBCT images reconstructed from the optimized trajectory with a sample non-optimized trajectory. The non-optimized trajectory was selected in the way to have a low value for the objective function in the ROI. The number of projections for the non-optimized trajectory was also selected to be the same as for the optimized trajectory in order to make the non-optimized trajectory comparable with the optimized trajectory. We realized the trajectories in the real situation with step-and-shoot protocol by placing the C-arm to each projection view. A standard circular CBCT scan from the C-arm device provided the ground truth for our experiments (Figs 3, 4 a). The C-arm CBCT scan included 313 projections and acquired over a 210° rotation and was reconstructed at a voxel size of 1 mm^3. The total number of projections and angulation selected for the optimized and non-optimized trajectories are given in Table I. The signs (+) and (-) denote rotation to the left/cranial and right/caudal directions, respectively. Reconstruction results for the optimized and non-optimized trajectories based on both real data and simulation data are shown in Figs. 3 (b, c) and 4 (b, c) respectively. Based on the results, the optimized trajectory shows very good visualization of the neck target. By contrast, images reconstructed from the non-optimized trajectory reveals poor visualization in ROI specially in the areas indicated by the red arrows. 3D visualization of the optimized and non-optimized trajectories compared to the circular trajectory is given in Fig. 5. For each of UQI and FSIM, the metric value between the C-arm CBCT and the reference CT from the head phantom was calculated and was called *Reference*. Furthermore, it was also computed between CBCT from optimized/non-optimized trajectories and the reference CT and was called *Measured*. Finally, we calculated the relative deviation between the *Reference* and *Measured* (Table II). According to the results, the relative deviation less than 10.31% for both metrics was achieved for the reconstructed image related to optimized trajectory while relative deviation for the non-optimized trajectory was found to be up to 48.31%. Our results demonstrate that the optimized trajectory has the potential to achieve a comparable image quality with respect to the reference C-arm CBCT for a given ROI while using a quarter of projections. The lower number of projections makes our optimized trajectory appropriate for low-dose CBCT interventions. In addition, compared to the C-arm circular CBCT with 210°angular range, our optimized trajectory uses a limited-angle view data with 156° angular rang which is 54° less than the C-arm CBCT.

TABLE I. THE SELECTED ANGULATIONS AND TOTAL PROJECTION NUMBER FOR BOTH OPTIMIZED AND NON-OPTIMIZED TRAJECTORIES

Trajectory	Arc	Angle	Projection number per arc	Total projection number
Opt.	Arc 1	θ_1= +22:2:+90, ψ= +1	35	78
	Arc 2	θ_2= -45:2:+39, φ= -30	43	
Non-opt.	Arc 1	θ_1= -67:2:+7, ψ= -29	38	78
	Arc 2	θ_2= -26:2:+52, φ= -22	40	

Opt.=Optimized, Non-opt.=Non-optimized

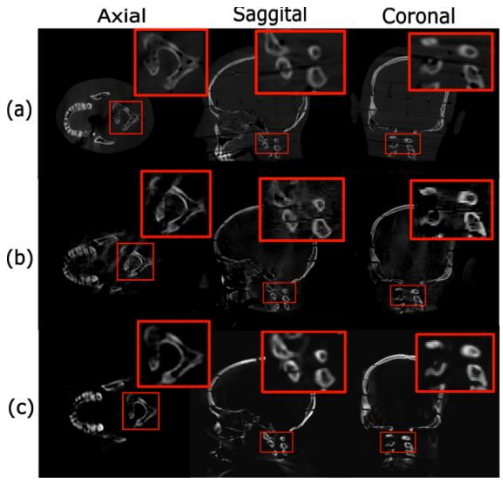

Figure 3. Reconstruction results for the neck target related to a) C-arm CBCT, b) optimized trajectory based on the real data, c) optimized trajectory based on the simulation data.

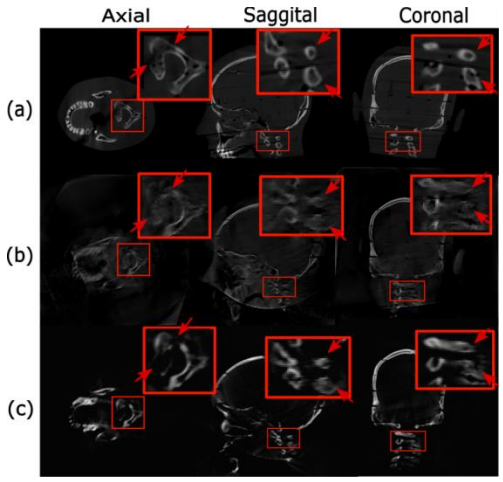

Figure 4. Reconstruction results for the neck target related to a) C-arm CBCT, b) non-optimized trajectory based on the real data, c) non-optimized trajectory based on the simulation data.

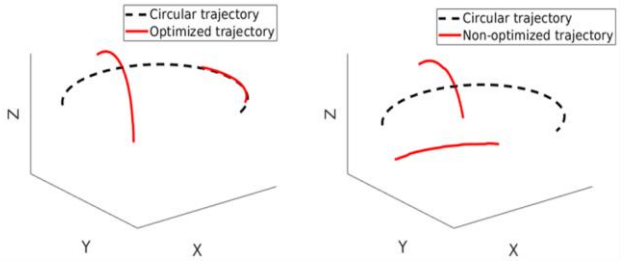

Figure 5. 3D visualization of the optimized/non-optimized trajectories with respect to the circular trajectory.

TABLE II. VALUES OF IMAGE QUALITY MEASURES UQI AND FSIM AND THEIR RELATIVE DEVIATION

Image quality metric	Trajectory	*Measured*	*Reference*	Relative deviation (%)
UQI	**Opt.**	0.70	0.79	10.31
	Non-opt.	0.41	0.79	48.31
FSIM	**Opt.**	0.74	0.80	7.54
	Non-opt.	0.60	0.80	25.41

IV. CONCLUSION

Within a realistic clinical scenario we demonstrated that applying a short-scan trajectory with a minimal set of projections and optimized orientations in 3D space is sufficient to localize the target and has a potential for low-dose CBCT-based interventions. In addition, our proposed optimized trajectory is a good suit for the limited angle CBCT reconstruction.

V. ACKNOWLEDGMENT

This work has been supported by ACMIT – Austrian Center for Medical Innovation and Technology, which is funded within the scope of the COMET program and funded by Austrian BMVIT and BMWFW and the governments of Lower Austria and Tyrol. We also gratefully acknowledge the support of NVIDIA Corporation for the donation of Titan Xp GPU used for this research.

REFERENCES

[1] D. A. Jaffray et al., "A radiographic and tomographic imaging system integrated into a medical linear accelerator for localization of bone and soft-tissue targets," *Int J Radiat Oncol Biol Phys*. 1999, vol. 45, pp. 773–89.

[2] M. W. Kan et al., "Radiation dose from cone beam computed tomography for image-guided radiation therapy," *Int J Radiat Oncol Biol Phys*. 2008, vol.70, pp. 272-279.

[3] J. W. Stayman and J. H. Siewerdsen, "Task-based trajectories in iteratively reconstructed interventional cone-beam CT," *The 12th Int'l Mtg. Fully 3D Image Recon. in Radiology and Nuc. Med.*, 2013, Lake Tahoe, June 16-21.

[4] J. W. Stayman, S. Capostagno, G. J. Gang, J. H. Siewerdsen, "Task-driven source–detector trajectories in cone-beam computed tomography: I. Theory and methods, " *J Med Imaging*. 2019, vol. 6(2):025002.

[5] S. Capostagno, et al., "Task-driven source–detector trajectories in cone-beam computed tomography: II. Application to neuroradiology," *J Med Imaging*. 2019, vol. 6(2): 025004.

[6] S. Hatamikia, A. Biguri, G. Kronreif, H. Furtado, J. Kettenbach, M. Figl, W. Birkfellner, "Source-detector trajectory optimization for C-arm CBCT", *Supplement of the International Journal of CARS (IJCARS)*, June 18 - 21, 2019, Rennes, France.

[7] S. Hatamikia, A. Biguri, L. Shiyamsundar, G. Kronreif, J. Kettenbach, W. Birkfellner, "Optimized Orientations for Target-based C-arm CBCT Reconstruction", *European Congress of Radiology* 2019. Vienna, Austria.

[8] T. Russ, A. M. Abdelrehim, D. F. Bauer, S. Hatamikia, L. Schad, F. Zöllner, K. Chung, "CBCT image quality and dose simulations for arbitrary source-detector trajectories with GATE", *European Congress of Radiology* 2020, Vienna, Austria.

[9] A. Biguri et al., "TIGRE: a MATLAB-GPU toolbox for CBCT image reconstruction," *Biomed Phys Eng Express*. 2016, vol. 2, 055010.

[10] S. Hatamikia et al., "CBCT reconstruction based on arbitrary trajectories using TIGRE software tool," *Proceeding of the 19th joint conference on new technologies for Computer/Robot Assisted Surgery (CRAS)*.March 2019, Genova, Italy.

[11] Z. Wang et al., "Image quality assessment: from error visibility to structural similarity," *IEEE Trans Image Process*. 2004, vol.13, pp.600-612.

[12] E. Y. Sidky, K.M. Kao, X. Pan, "Accurate image reconstruction from few-views and limited-angle data in divergent-beam CT," *J. X-Ray Sci. and Technol.* 2009, vol. 14, pp. 119–139.

[13] Z. Wang, A. Bovik, "A universal image quality index," *IEEE Signal Proc Lett*. 2002, vol. 9, pp. 81-84.

[14] L. Zhang et al., "FSIM: A Feature Similarity Index for Image Quality Assessment. IEEE Trans Image Process," *IEEE Trans Image Process*. 2011, vol. 20, pp. 2378-2386.